Journal of Molecular Graphics and Modelling 29 (2010) 171–177

Contents lists available at ScienceDirect

Journal of Molecular Graphics and Modelling

journal homepage: www.elsevier.com/locate/JMGM

Structure-based design of carbon nanotubes as HIV-1 protease inhibitors: Atomistic and coarse-grained simulations

Yuan Cheng[a,*], Dechang Li[b], Baohua Ji[c], Xinghua Shi[d], Huajian Gao[d]

[a] Institute of High Performance Computing, 1 Fusionopolis Way, #16-16 Connexis, Singapore 138632, Singapore
[b] Department of Engineering Mechanics, School of Aerospace, Tsinghua University, Beijing 100084, China
[c] Biomechanics and Biomaterials Laboratory, Department of Applied Mechanics, Beijing Institute of Technology, Beijing 100081, China
[d] Division of Engineering, Brown University, Providence, RI 02912, USA

ARTICLE INFO

Article history:
Received 25 January 2010
Received in revised form 20 May 2010
Accepted 20 May 2010
Available online 27 May 2010

Keywords:
HIV-1 protease
Carbon nanotubes
Molecular dynamics
Atomistic model
Coarse-grained model

ABSTRACT

Nanoparticles such as fullerenes and carbon nanotubes have been extensively studied for biomedical applications. In this paper, we report the design of carbon nanotubes as HIV-1 protease inhibitors. Docking and molecular dynamics calculations are performed using an atomistic model to explore the optimal interaction structure and free energy between the nanotube and HIV-1 protease. A coarse-grained model is then developed based on the atomistic model, allowing us to investigate the dynamic behaviors of the protease in the bound and unbound states. The dynamic process reveals that the carbon nanotube is able to bind to the active site of the protease and prevent the active flaps from opening up, thus blocking the function of the protease. This process is strongly influenced by the size of the nanotube. The binding of carbon nanotubes to an alternative binding site other than the active site is also explored. Therefore, carbon nanotube-based inhibitors have great potential for application as HIV-1 protease inhibitors.

1. Introduction

HIV-1 protease (HIV-PR) has been one of the major targets in anti-AIDS drug discovery. Although a number of potent and selective inhibitors have been developed as drugs for the treatment of HIV infection, great efforts are still needed to explore more stable and effective inhibitors.

HIV-PR belongs to a family of aspartic acid proteases. This enzyme is composed of two 99-amino acid monomers, named monomer *A* and monomer *B* in this paper. The structure of the protease features a pair of flaps and the active site, where ILE50A and ILE50B are defined as flap tips, as shown in Fig. 1. The flaps constantly sample different states, the most populated of which are the closed, semi-open, and open states. In the open state of the protease, the flap tip distance reaches up to 20–30 Å [1]. Experimental NMR data have shown that the large-scale flap motions occur on the microsecond–millisecond timescale [2]. The active site of this enzyme can be roughly described as an open-ended cylindrical tube that is lined almost exclusively by hydrophobic amino acids [2,3] and that cleaves polypeptides involved in the generation of the mature HIV virus. Once the polypeptides enter the active site through the opened flaps, the flaps close up to allow the protease to function. HIV-PR inhibitors function by controlling the flap dynamics and blocking the pathway of polypeptides entering the active site.

Among the different types of HIV-PR inhibitors, nanoparticles possess several advantages over conventional peptide-based inhibitors. First, compared to peptide-based inhibitors, nanoparticles are stable and do not easily react with other chemical compounds [3]. Second, nanoparticles such as C_{60} and carbon nanotubes (CNTs) are rigid and tend to retain their geometrical structure, and therefore, they are expected to effectively interact with non-polar chemical motifs [4]. The inhibition effect of fullerene derivatives has been investigated via computational and experimental approaches. For example, experimental studies have shown that fullerene C_{60}-derivatives can be very effective inhibitors, with an inhibition constant K_i ~100 nM [4–7]. Furthermore, fullerene drugs in human PBM, Vero or CEM cells at concentrations of up to ~100 μM are non-cytotoxic [8]. These results indicate that fullerene C_{60}-based inhibitors are promising to be utilized as drugs [3–10]. Enzyme inhibition by fullerene-based compounds has also been found for nitric oxide syntheses [10,11] and glutathione reductase [12]. Based on previous work, the assumptions of our present study are that CNT-based ligands can also serve as effective inhibitors and have advantages over conventional inhibitors owing to their geometrical and chemical properties. The geometry of the CNTs is expected to

* Corresponding author. Tel.: +65 64191252.
E-mail addresses: chengy@ihpc.a-star.edu.sg, chengyuan523@gmail.com (Y. Cheng).

1093-3263/$ – see front matter © 2010 Elsevier Inc. All rights reserved.
doi:10.1016/j.jmgm.2010.05.009

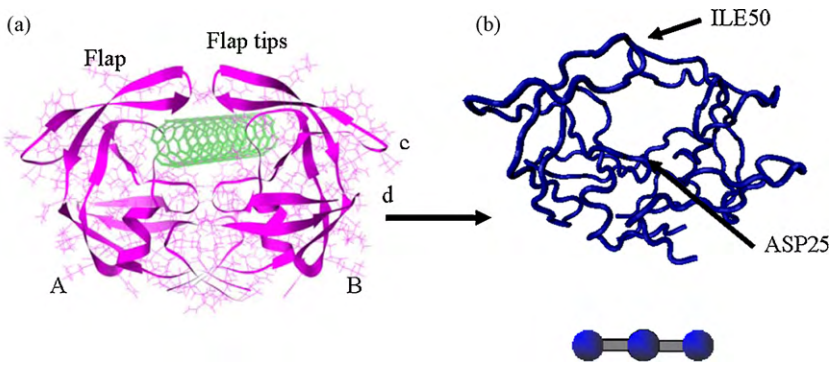

Fig. 1. (a) Configuration of the SWCNT–protease complex. (b) CG model for HIV-PR and SWCNT, respectively. The pictures were generated using the UCSF Chimera package [40] and VMD [41], respectively.

complement the active cavity of the protease even better than C_{60}.

All-atom models have been a powerful tool in the exploration of interactions between enzymes and their inhibitors [3,5,13,14]. For example, Friedman et al. [3] studied the inhibition of HIV-PR by fullerene derivatives, showing that functionalized C_{60} could serve as an effective, high affinity HIV-PR inhibitor through careful design.

However, the timescales of inhibitors entering the active site, as well as the dynamic behaviors of the protease, are not accessible to all-atom models. Therefore, the development of coarse-grained (CG) models is also crucial for understanding the dynamic behaviors of the enzyme. In the present work, an all-atom model was developed to determine the optimal interaction structure of the complex of a single-walled carbon nanotube (SWCNT) and the protease through docking. A molecular dynamics (MD) simulation was carried out to evaluate the binding free energy between CNT and the protease. A CG model of HIV-PR was also adopted for the simulation of CNT binding dynamics. The CG model was first developed by McCammon and co-worker [15]. The model has been successfully adopted to study the dynamic behaviors of HIV-PR and the binding pathways of ligands to the protease [16], which allows one to obtain the μs timescale to simulate the flap opening dynamics. We further incorporated the simplified model of the SWCNT into the CG system, with the CNT–protease interaction parameters determined based on the results of the all-atom model. Dynamic simulation results suggest that the CNT may enter the active site of the protease without flap opening and is able to prevent the flap from opening. Binding of the CNT to alternative target sites other than the active site was also observed, indicating the control of dynamic behaviors of the protease through allosteric effects.

By integrating the simulation results based on different molecular level resolutions, this paper proposes a general approach to designing nanoparticle-based inhibitors according to the geometrical properties of the enzyme.

2. Methods

2.1. Modeling the CNT–protease complex through docking

The docking algorithm was used to find the optimal configuration of the CNT inside the active site of the protease. The structure of the ligand-free HIV-PR was obtained from the protein data bank (entry: 1HHP [17]). A (5, 5) SWCNT with a diameter of 6.8 Å and a length of 24.0 Å was selected as a candidate for the inhibitor. Force field AMBER99 [18] was used throughout the simulation. The parameters for carbon atoms on CNTs were taken from type CA in the AMBER99 force field, and these parameters are designed for aromatic carbon atoms. The software package SYBYL 8.0 (Tripos Associates, Inc., St. Louis, USA) was used for modeling the molecular structure. Initially, the SWCNT was placed inside the active site of the protease, and the docking algorithm was carried out using the software package DOCK6 [19].

To model the optimal CNT–protease interaction configuration, molecular surface areas were determined from molecular surfaces generated by the program DMS (Conrad Huang, University of California, San Francisco, USA). The default van der Waals (VDW) radii and a probe sphere diameter of 1.4 Å were used. The 28 spheres surrounding the active site were generated. Using docking, the optimal orientations of a ligand inside the binding pocket could be found by scoring the energy based on the VDW contacts and complementary electrostatics. Therefore, the grid-based score was generated by calculating the non-bonded terms of the molecular mechanic force field, and the structure with the highest score was then adopted for MD simulation. A representative SWCNT–protease complex configuration is shown in Fig. 1a.

2.2. MD simulation

2.2.1. MD simulation in explicit solvent

Atomistic MD simulation was carried out using the software AMBER 8.0 [20]. To prepare the system for the binding free energy calculation in the next stage, MD simulations were performed on the CNT, the HIV-PR, and the CNT–protease complex, with each object solvated in a TIP3P water box. A layer of 8 Å of water molecules was applied in all three directions surrounding the solute, and the periodic boundary condition was used on all sides. For each system, 20,000 cycles of energy minimization were carried out, followed by 4 ns of MD simulation. The temperature of the system was heated from 100 K to 300 K during the first 200 ps using a constant volume and constant temperature (NVT) ensemble. Afterwards, the system was kept at room temperature of 300 K and a pressure of 1 bar using a constant pressure and constant temperature (NPT) ensemble [21]. The stability of the simulation was tracked, and the structure was prepared for the free energy calculation in the next stage.

2.2.2. Calculating the interaction free energy using the molecular mechanics-general Borned surface area (MM-GBSA) method

Water molecules from the previous equilibrated systems were removed, and the binding free energy between the protease and the SWCNT was calculated using the MM-GBSA method, where the GB model is the pairwise generalized Born model (GB^{HCT}) by Hawkins et al. [22,23], with parameters described by Tsui and Case [24]. The simulation was carried out for 500 ps for equilibrium and 500 ps for data collection. Here, the binding free energy was determined as the energy difference between the free energies of the complex in the implicit water solvent ($G^{solvate}_{complex}$) and the sum of the SWCNT

($G^{solvate}_{nanotube}$) and the protease ($G^{solvate}_{pro}$) solvated in water.

$$\Delta G = G^{solvate}_{complex} - (G^{solvate}_{nanotube} + G^{solvate}_{pro}). \quad (1)$$

For each system, the absolute value of the free energy was determined by its molecular mechanics energy in a vacuum, E_{vac}, and the solvation free energy $G_{solvation}$.

$$G = E_{vac} + G_{solvation}. \quad (2)$$

According to molecular mechanics theory, E_{vac} was calculated as

$$E_{vac} = E_{internal} + E_{vdw} + E_{ele}, \quad (3)$$

where E_{vac} is composed of the internal energy ($E_{internal}$), the van der Waals interaction energy (E_{vdw}), and the electrostatic energy (E_{ele}).

The internal energy includes the bond stretching, the angle bending, and the torsion energy, which can be further expressed as

$$E_{internal} = E_{bond} + E_{angle} + E_{torsion}. \quad (4)$$

The solvent-induced free energy $G_{solvation}$ involves both polar and non-polar terms:

$$G_{solvation} = G_{pol} + G_{nonpol}. \quad (5)$$

Here, the polar term is calculated using

$$G_{pol} = \sum_{ij}^{atoms} \frac{q_i q_j}{f^{gb}(R_{ij})}, \quad (6)$$

where the function f^{gb} estimates the reaction field potential [24]. The surface area of the solute was computed using the linear combinations of pairwise overlaps (LCPO) model, with $\sigma = 0.0072$ kcal/mol Å^2 [25,26].

$$G_{nonpol} = \sigma A. \quad (7)$$

Therefore, the binding free energy is composed of several energetic terms and is summarized by

$$\Delta G = \Delta E_{vac} + \Delta G_{solvation} = \Delta E_{internal} + \Delta E_{vdw} + \Delta E_{ele} + \Delta G_{pol} + \Delta G_{nonpol}. \quad (8)$$

2.2.3. Calculating the interaction free energy using the molecular mechanics-Poisson–Boltzmann solvation area (MM-PBSA) method

We have also performed MM-PBSA calculation to evaluate the CNT–protease binding free energy and single trajectory approach was carried out based on MD simulation results. The binding free energy is calculated as follows

$$\Delta G = \Delta E_{vac} + \Delta G_{solvation} = \Delta E_{ele} + \Delta E_{vdw} + \Delta G_{pol} + \Delta G_{nonpol}, \quad (9)$$

where ΔE_{vdw} and ΔE_{ele} are the van der Waals energy and electrostatic energy difference between two states, respectively. There is no change in electrostatic energy since the CNT carries no charge. The energy ΔG_{pol} denotes the polar solvation energy, which was calculated numerically by solving the Poisson–Boltzmann equations using the APBS package [27]. The grid size was set at 0.5 Å, and the interior dielectric constant was set at 1.0 while the dielectric constant of water was taken to be 80. The radii of atoms were taken from the AMBER parameters set by the PDB2PQR service [28]. The non-polar contribution corresponded to the burial of the solvent-accessible surface area (SASA) upon binding, which were calculated by

$$\Delta G_{nonpol} = \gamma \times SASA + \eta. \quad (10)$$

where SASA was the solvent-accessible surface area, which was calculated by the MSMS program [29] with 1.4 Å radius probe sphere; the constant γ was set at 0.00542 kcal/(mol Å^2), and η at 0.92 kcal/(mol) [30,31].

2.3. CG model and Langevin dynamics (LD)

The CG model for HIV-PR adopted in this work was first developed by McCammon and co-worker [15]. In this model, each amino acid residue is represented by one CG bead, and each bead with a different size and weight is placed at the C_α position of the corresponding residue. These beads are connected by pseudo-bonds, angles and dihedral angles. The potential energy function of the ligand-free system was calculated as the sum of all the energy components as follows:

$$U = U_{bond} + U_{angle} + U_{dihedral} + U^{non\text{-}local}_{elec} + U^{local}_{nb} + U^{non\text{-}local}_{nb}, \quad (11)$$

where U_{bond}, U_{angle}, and $U_{dihedral}$ are bonded intramolecular interactions terms [14]; $U_{elec} = q_i q_j / \varepsilon r_{ij}$ denotes the Coulombic interaction, where r_{ij} is the distance between the beads i and j; q_i and q_j denote the charges on the particles. A distance-dependent dielectric coefficient ($\varepsilon_{ij} = 4r_{ij}$) was adopted to avoid unrealistic in vacuo Coulombic interactions [16]. The inhibitor CNT is modeled as a neutral ligand and does not carry charges. The local and non-local non-bonded intramolecular interaction functions, U^{local}_{nb} and $U^{non\text{-}local}_{nb}$, are defined in a form of Morse potential during the dynamics simulation. The local non-bonded interactions are allowed to break, and non-local interactions can form during the simulation, which is determined using the distance between two beads.

$$U_{nb} = \begin{cases} U^{local}_{nb} = \beta\left[(1 - e^{-\alpha(r_{ij} - r_0)})^2 - 1\right] & r_{ij} \le 8\ \text{Å} \\ U^{non\text{-}local}_{nb} = 0.20708\left[(1 - e^{-\alpha(r_{ij} - 9.75)})^2 - 1\right] & 8\ \text{Å} \le r_{ij} \le 15\ \text{Å} \end{cases}, \quad (12)$$

where r_{ij} is the distance between two beads, and r_0 is the value at equilibrium within the critical distance 8 Å, which is calculated according to the average semi-open state of the protease (PDB code 1HHP, for example); α and β are fitting parameters, where $\alpha = 0.70711$ Å^{-1} and $\beta = 6$ exp $(-r_0/2.8)$ kcal/mol [32]. The initial configuration of HIV-PR was constructed based on the semi-open structure of the protease with PDB entry 1HHP, as shown in Fig. 1b.

The CG model of the SWCNT was constructed using three beads connected by pseudo-bonds, and the SWCNT was simplified as one rigid beam. The effective radius of each bead was 3.5 Å, and the bond connecting the beads was set at 8.5 Å in length with a spring constant of 300 kcal/(mol Å^2). The angle was maintained at 180° with a constant of 2 kcal/(mol rad^2). The simplified model qualitatively reproduces the geometric properties of the nanotube.

The interactions between HIV-PR and the inhibitors are described by a modified Lennard–Jones potential [16,33]:

$$U^{inter}_{vdw} = \varepsilon_0 \left[\left(\frac{R_i + R_j}{r_{ij}} \right)^8 - 1.5 \left(\frac{R_i + R_j}{r_{ij}} \right)^6 \right], \quad (13)$$

where r_{ij} is the distance between bead i and j, while R_i and R_j are the effective radii of bead i in the protease and bead j in the inhibitor, respectively. The cut-off for calculating the intermolecular interactions between the CNT and the protease is set at 20 Å.

The CG simulations were carried out using the software package Gromacs 3.3.1. Langevin dynamics (LD) is performed to mimic the frictional and stochastic effects of the solvent.

$$m_i \frac{d^2 r_i}{dt^2} = F_i(r) - \xi_i m_i \frac{dr_i}{dt} + R_i(t), \quad (14)$$

where m_i is the mass of the bead in the CG model, r_i is the coordinate of the bead at instantaneous time, $F_i(r)$ is the force on the bead, ξ_i is the friction constant and a value of $2/ps$ is adopted, and $R_i(t)$

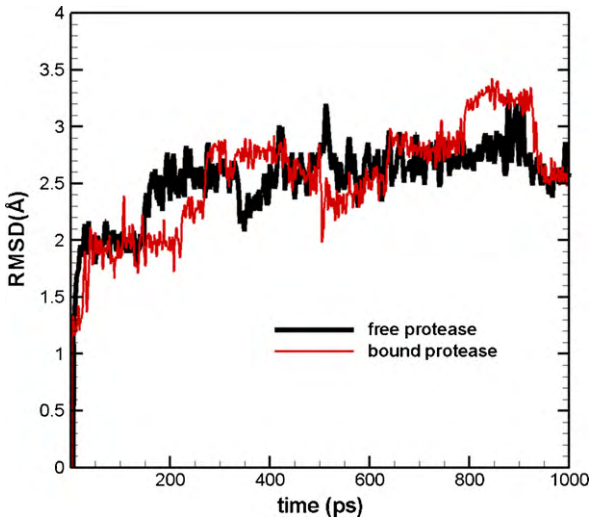

Fig. 2. Root mean square deviation (RMSD) of C_α atoms on bound and free HIV-PR during MD simulation.

is the random noise term that satisfies $\langle R_i(0)R_j(t)\rangle = 2m_i\gamma k_B T\delta_{ij}(t)$, where k_B is the Boltzmann constant and T is the temperature. A time step of 10 fs was used to integrate the equation of motion, which was proven appropriate for simulating the CG system [34]. The non-bonded pair list was updated every 5 steps, and the interaction cut-off between the CG beads of the protease and the inhibitors was set at 20 Å. The size of the CNT could be controlled by varying the diameter of the effective radii and the number of beads constituting the CNT.

3. Results and discussion

3.1. All-atom MD simulations

Atomistic MD simulations are performed to study ligand–receptor interactions at equilibrium. In this work, the optimal structure of the SWCNT interacting with HIV-PR was obtained through docking and was then subjected to MD simulation for equilibrium and data collection. The root mean square deviation (RMSD) of the C_α protease in the bound and unbound states in MD simulation is plotted in Fig. 2. Overall, the structure of the protease was stable without unreasonable oscillation. As shown in Fig. 1a, the cylindrical shape of the SWCNT shows a complementary fitting with the geometry of the active site of the protease.

The binding free energy of the SWCNT to the protease and all of the energy components calculated using MM-GBSA method are listed in Table 1. Detailed energetic contributions of CNT–protease interactions using MM-GBSA method are provided in Table S1 in supplementary data. During the simulation, the energies fluctuated within standard errors, and the contribution of the internal energy was not significant. The in vacuo electrostatic energy change (ΔE_{ele}) and the solvent-induced polar free energy (ΔG_{pol}) tend to cancel each other out; the sum of the two terms is shown as ΔE_{ele_total}. Therefore, the VDW interaction contributes dominantly to the binding between the CNT and the protease, which is consistent with previous studies [3,5]. The calculation yields a binding free energy of −120.55 kcal/mol, indicating a strong affinity of the SWCNT for HIV-PR.

As a comparison with the GBSA method, MM-PBSA calculation has also been performed [35] based on single trajectory approach [36,37]. The free energy calculated using MM-PBSA method is −163.07 kcal/mol, and the energetic contributions are also shown in Table 1. It is shown that both GBSA and PBSA methods yielded qualitatively comparable results. In the present case, the CNT carries no charge, and the VDW interaction dominates the CNT–protease interaction, therefore different approaches do not influence the results significantly.

Table 1
Energetic contributions of CNT–protease interactions using MM-GBSA and MM-PBSA methods.

	MM-GBSA (kcal/mol)	MM-PBSA (kcal/mol)
$\Delta E_{internal}$	17.92 ± 47.46	[b]
ΔE_{ele}	−246.66 ± 460.20[a]	[b]
ΔE_{vdw}	−146.32 ± 31.30	−164.88 ± 33.08
ΔG_{pol}	258.81 ± 453.51[a]	12.53 ± 3.14
ΔG_{nonpol}	−4.58 ± 2.52	−10.72 ± 0.23
ΔG	−120.55 ± 29.26	−163.07 ± 33.35

[a] These components are due to the charge distribution changes of HIV-1 PR itself since the CNT carries no charge. These two components tend to cancel each other out; the sum of the two terms is 12.14 kcal/mol (see Table S1), which is consistent with ΔG_{pol} value calculated by MM-PBSA method.
[b] There are no contributions of these components since single trajectory approach was adopted. There is no change in electrostatic energy because the CNT does not carry any charge.

Although the atomistic simulation provides great insights into the mechanism of the ligand–receptor interaction at high resolution, the dynamic behavior of the protease can only be observed over a much longer timescale, which requires the development of a CG model.

3.2. CG model and dynamic binding process

3.2.1. Dynamics of the ligand-free protease and CNT binding mechanism

The CG model adopted in this work has been validated in earlier work [15,34]. In our simulation of the ligand-free HIV-PR, the protease constantly samples the open, semi-open, and close states. These different states are defined according to the topology of the protease. The open state of HIV-PR is defined when a correlated opening of the ILE50A–ILE50B is larger than 14 Å and ASP25A–ILE50A is larger than 18 Å, i.e., when the two distances occur simultaneously [34]. Here, ILE50A–ILE50B denotes the distance between ILE50 on monomer *A* and ILE50 on monomer *B*. The root mean square fluctuation (RMSF) of all the residues on the protease is shown in Fig. 3a, indicating a larger fluctuation near the flap tips ILE50A and ILE50B, as compared to other regions. The opening dynamics of the flap tips as a function of the simulation time is also shown in Fig. 3b. For the ligand-free protease without constraint, the ILE50A–ILE50B distance constantly reaches the peak value, corresponding to the open state of the flaps. Therefore, the CG model is capable of reproducing the dynamic behavior of the ligand-free protease, including the fluctuations, collectivity, and flexibility of the structure.

The binding process of the CNT to HIV-PR was also studied. To match the CNT–protease interaction free energy of the all-atom model, ε_0 = 0.66 kcal/mol was adopted as the non-bonded interaction parameter in Eq. (13). The LD simulation was performed for several cycles with the CNT located at different initial positions outside the active pocket of the HIV-PR. The initial structure of the HIV-PR was semi-open and the protease was unconstrained throughout the simulation. It was found that the binding pathway of the CNT to the protease is sensitive to the initial configuration. One representative process of a CNT entering the protease is shown in Fig. 4. Initially, the CNT was located approximately 2 nm away from the active site of the protease, with no direct contact with the protease surface. During the simulation, the CNT gradually approaches the protease and rotates toward a favorable orientation for insertion into the cavity of the active site.

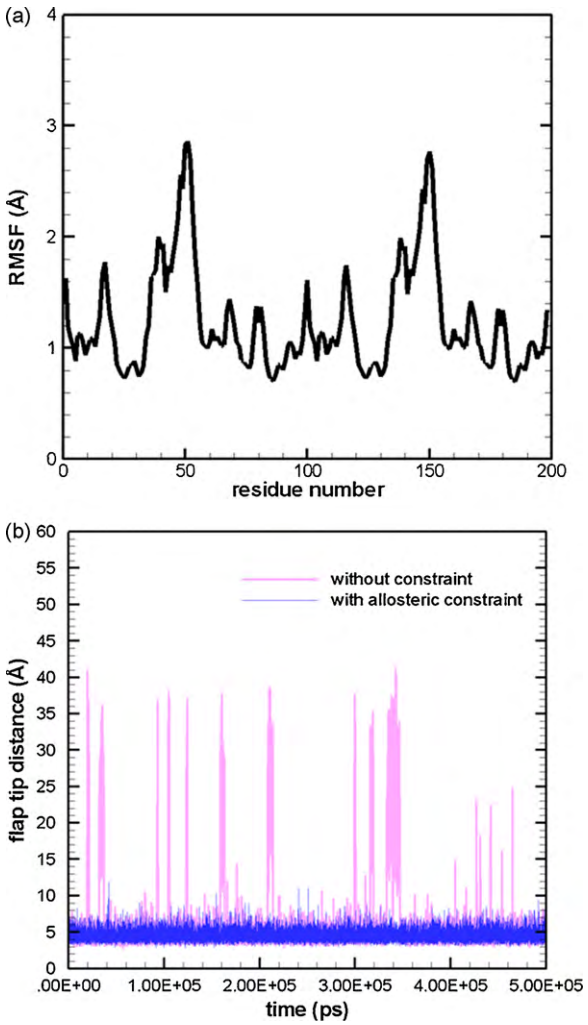

Fig. 3. Dynamic behavior of the ligand-free protease using the CG model. (a) Root mean square fluctuation (RMSF) of the ligand-free HIV-PR. (b) Flap tip distance of the ligand-free HIV-PR as a function of simulation time with/without allosteric constraints on residues 15–19, 35–42 (cheek sheet).

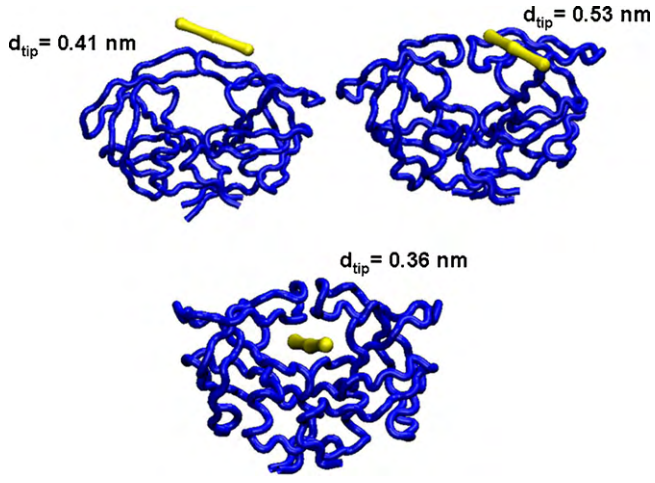

Fig. 4. Snapshots of CNT–protease interactions at 0 ns, 0.8 ns, and 2 ns. The pictures were produced using VMD. The flap tip distance (d_{tip}) was also illustrated.

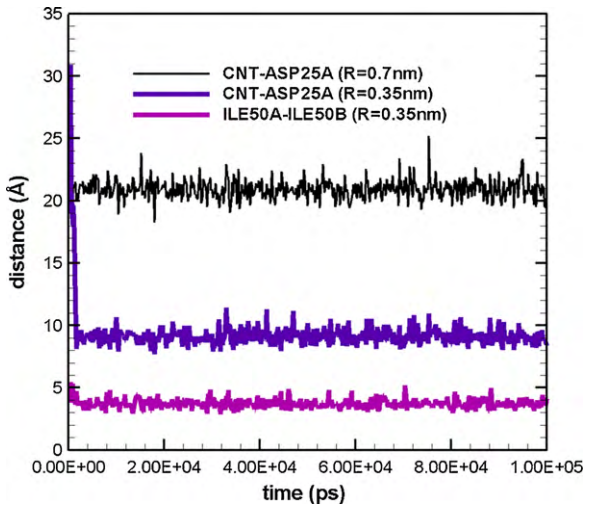

Fig. 5. Binding processes of CNTs to the protease, with a CNT diameter of $R = 0.7$ nm and $R = 0.35$ nm.

The binding process of the CNT as it enters the active site of the protease is quantitatively shown in Fig. 5. The center of mass (COM) distance between the CNT and ASP25A shows that the binding process is completed within 20 ns. The corresponding flap dynamics are also illustrated in Fig. 5. The ILE50A–ILE50B distance with respect to the simulation time indicates that the CNT can bind to the active site without opening the flaps. It has been shown in previous work that inhibitors with a small size, e.g., XK263, can enter the cavity even when the flaps are closed [34]. Due to the small size of the CNT, it is therefore reasonable that the CNT enters the active site without requiring flap opening. This observation is also consistent with a one-step 'diffusion control' mechanism [38].

After binding to the active site, the CNT remains inside the active site and does not escape during the simulation time of 500 ns. The flap of the protease is stabilized by the CNT and does not open during the simulation up to 500 ns (only the data during the first 100 ns is illustrated in the figure). Therefore, the CNT can effectively inhibit the function of the protease through geometrical constraint.

The variation of non-bonded interaction energy between the protease and the CNT against the simulation time is also shown in Fig. 6, where an average energy of -114.9 ± 3.11 kcal/mol is observed. Equilibrium data collection is carried out after 40 ns. The

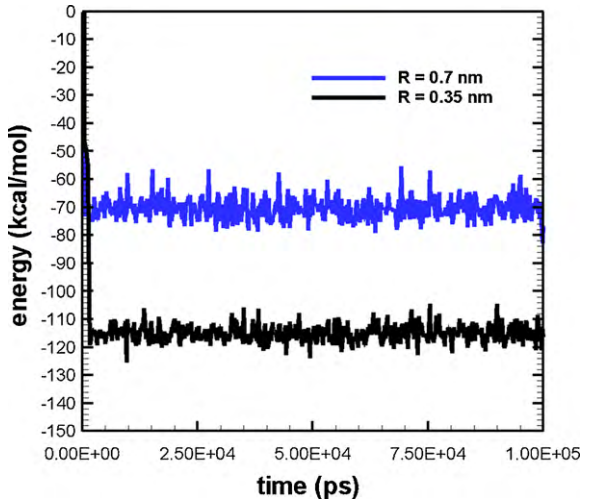

Fig. 6. Non-bonded interaction energy between CNTs and the protease with respect to simulation time. Two cases with a CNT diameter of $R = 0.7$ nm and $R = 0.35$ nm were investigated.

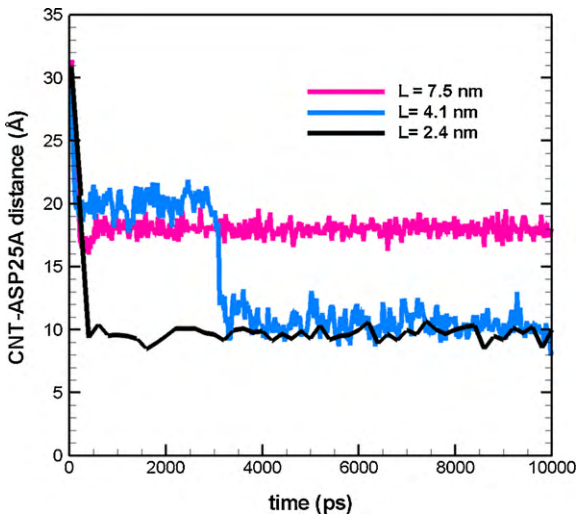

Fig. 7. Binding processes of CNTs to the protease, with CNT length varying from $L = 2.4$ nm to $L = 7.5$ nm.

strong affinity of the CNT for the protease facilitates the fast binding process.

The CNT–protease binding mechanism was further investigated by simulating binding process of the CNT to an open state HIV-PR. It is shown that the CNT enters the active site of the protease rapidly, and the flap closes up after the CNT enters the active site of the protease.

3.2.2. CNT size effect on the binding process

The size of inhibitors plays a substantial role in their ability to bind to the active site of the protease. Friedman et al. designed fullerene derivatives as inhibitors of HIV-PR through computational docking and experimental studies [3]. In the present work, we show that a (5, 5) type of CNT with a comparable diameter to C_{60} is appropriate to serve as the HIV-PR inhibitor. If a CNT with a larger diameter, e.g., an (8, 8) SWCNT, is used, the binding process is significantly hindered, as shown in Figs. 5 and 6. The CNT may fail to enter the cavity of the protease. The diameter of a CNT is varied by controlling R_j in Eq. (13). Other parameters in the simulation remain unchanged.

The effect of CNT length was also investigated. For example, a very short CNT resembles a fullerene, which is allowed to rotate inside the active cavity. Compared to short CNTs, it takes a longer time for a long CNT to orient toward a favorable configuration for entering the binding pocket; therefore, the binding process is less efficient. The binding processes of CNTs with different lengths to the protease are compared in Fig. 7. Initially, the COM of the CNTs is located at the same position in these systems, while different numbers of particles are adopted to construct the CG model of CNTs with different lengths. Longer CNTs may even attach to the surface of the protease instead of entering the cavity.

3.2.3. Elbow regions targeted as the alternative binding site

In addition to the active site, elbow regions were also studied as alternative binding sites for drug targets using the CG model. The elbow region on the protease is defined as 17-turn and 39-turn, corresponding to the "c" and "d" sites illustrated in Fig. 1a. Previous CG simulation with allosteric constraint on the elbow region indicated an anti-correlation of the c–d distance with the flap tip distance [15]. As shown in Fig. 3b, the flap on the HIV-PR is prevented from opening if residues 15–19 and 35–42 are constrained.

Lexa et al. showed that in the crystal structure of a multidrug-resistant HIV-PR (PDB entry 1TW7), peptides were only interacting with but were not tightly bound to the elbow site [39]. We hypothesize that compared to peptide-based ligands, CNTs have a relatively stronger affinity for HIV-PR due to the VDW interaction, implying a tight binding of the CNT not only to the active site but also to the elbow site. Based on this hypothesis, we located two CNTs near the elbow regions and ran LD for 200 ns until each CNT bound to one side on the elbow region of the protease, respectively. The structure and energetic data shown in Fig. 8a and b were collected after the system reached equilibrium.

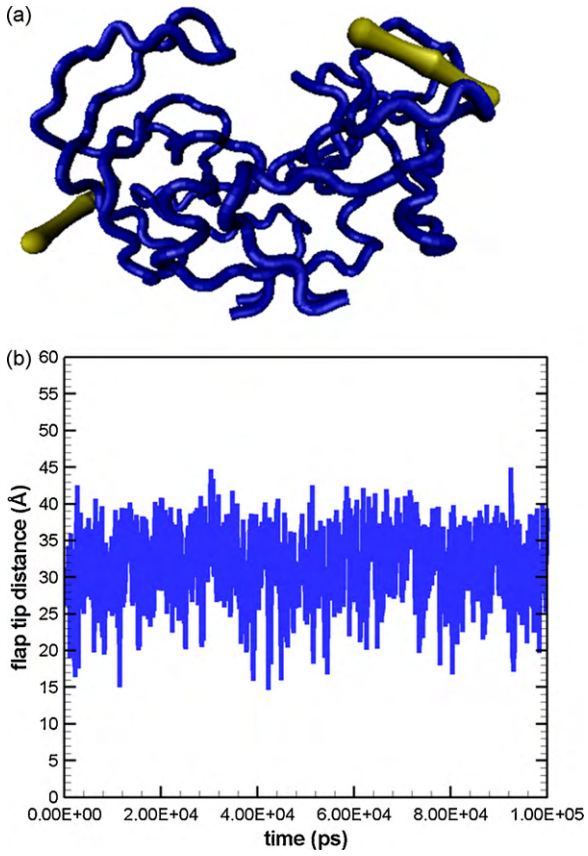

Fig. 8. (a) Snapshots of two CNTs (yellow) docked to the elbow site of HIV-PR. (b) Flap tip distance as a function of the simulation time when two CNTs are inside the elbow site. (For interpretation of the references to colour in this figure legend, the reader is referred to the web version of the article.)

The flap tip distance as a function of the simulation time is shown in Fig. 8b, indicating that the docking of two CNTs to the elbow region of the protease does not prevent the flaps from opening. Instead, the flaps remain open. This finding could be explained by previous observations that the correlation between the c–d distance and the flap tip distance is opposite when the flaps are in the very open conformation. In this work, the allosteric effect of docking two CNTs onto the elbow region caused a wider opening between site "c" and "d", and the flap tip distance increased, which is similar to the inhibition effect observed when the flaps are widely opened and the elbow sites are constrained, preventing the flaps from closing.

Binding of rigid nanoparticles to the elbow region demonstrate an alternative way to control the dynamic behaviors of HIV-PR through allosteric constraint. By controlling flap movements, the function of HIV-PR can be deactivated.

4. Conclusions

In summary, we have explored the application of CNTs as HIV-PR inhibitors through structure-based design. CNTs have a strong affinity for HIV-PR due to their geometrical complimentarily to,

and strong VDW interaction with, the active site of the protease. The docking algorithm and free energy calculations were carried out using the all-atom model. A CG model was further developed to reveal the binding process of the CNT as it enters the binding cavity of HIV-PR. We showed that the CNT could effectively prevent the flaps from opening after binding to the active site. The size effect of the CNTs on the binding mechanism was investigated. We also showed that the binding of CNTs to alternative binding sites helped to control the dynamic behaviors of the protease. This study proposes a general guideline for the design of nanoparticle-based enzyme inhibitors via different levels of model resolution.

Acknowledgments

This work reported was supported by the A*Star Visiting Investigator Program "Size Effects in Small Scale Materials" hosted at the Institute of High Performance Computing in Singapore. We gratefully acknowledge the contributions of Dr. Chun Lu and Prof. Yongwei Zhang, who provided helpful management and discussions during the course of the work. Y.C. wishes to thank Dr. Bing Zhang from Research Centre of Excellent in Mechanobiology, National University of Singapore for helpful discussions. B.J. would like to acknowledge the support by the National Natural Science Foundation of China through Grant Nos. 10628205, 10732050, and 10872115.

Appendix A. Supplementary data

Supplementary data associated with this article can be found, in the online version, at doi:10.1016/j.jmgm.2010.05.009.

References

[1] V. Hornak, A. Okur, R.C. Rizzo, C. Simmerling, HIV-1 protease flaps spontaneously open and reclose in molecular dynamics simulations, Proc. Natl. Acad. Sci. U.S.A. 103 (2006) 915–920.
[2] R. Ishima, D.I. Freedberg, Y.X. Wang, J.M. Louis, D.A. Torchia, Flap opening and dimer-interface flexibility in the free and inhibitor-bound HIV protease, and their implications for function, Structure 7 (1999) 1047–1055.
[3] S.H. Friedman, D.L. DeCamp, R.P. Sijbesma, G. Srdanov, F. Wudl, G.L. Kenyon, Inhibition of the HIV-1 protease by fullerene derivatives: model building studies and experimental verification, J. Am. Chem. Soc. 115 (1993) 6506–6509.
[4] S.H. Friedman, P.S. Ganapathi, Y. Rubin, G.L. Kenyon, Optimizing the binding of fullerene inhibitors of the HIV-1 protease through predicted increases in hydrophobic desolvation, J. Med. Chem. 41 (1998) 2424–2429.
[5] Z.W. Zhu, D.I. Schuster, M.E. Tuckerman, Molecular dynamics study of the connection between flap closing and binding of fullerene-based inhibitors of the HIV-1 protease, Biochemistry 42 (2003) 1326–1333.
[6] S. Bosi, T. Da Ros, G. Spalluto, M. Prato, Fullerene derivatives: an attractive tool for biological applications, Eur. J. Med. Chem. 38 (2003) 913–923.
[7] O. Aruksakunwong, S. Promsri, K. Wittayanarakul, P. Nimmanpipug, V.S. Lee, A. Wijitkosoom, P. Sompornpisut, S. Hannongbua, Current development on HIV-1 protease inhibitors, Curr. Comp. Aid. Drug Des. 3 (2007) 201–213.
[8] R.F. Schinazi, R. Sijbesma, G. Srdanov, C.L. Hill, F. Wudl, Synthesis and virucidal activity of a water-soluble, configurationally stable, derivatized C60 fullerene, Antimicrob. Agents Chemother. 37 (1993) 1707–1710.
[9] F.N. Steinmetz, et al., Buckyballs meet viral nanoparticles: candidates for biomedicine, J. Am. Chem. Soc. 131 (2009) 17093–17095.
[10] H. Benyamini, A. Shulman-Peleg, H.J. Wolfson, B. Belgorodsky, L. Fadeev, M. Gozin, Interaction of C_{60}-fullerene and carboxyfullerene with protein: docking and binding site alignment, Bioconjug. Chem. 17 (2006) 378–386.
[11] D.J. Wolff, C.M. Barbieri, C.F. Richardson, D.I. Schuster, S.R. Wilson, Trisamine C(60)-fullerene adducts inhibit neuronal nitric oxide synthase by acting as highly potent calmodulin antagonists, Arch. Biochem. Biophys. 399 (2002) 130–141.
[12] T. Mashion, K. Okuda, T. Hirota, M. Hirobe, T. Nagano, M. Mochizuki, Inhibitory effect of fullerene derivatives on glutathione reductase, Fullerene Sci. Technol. 9 (2001) 191–196.
[13] B. Zhang, V.B.C. Tan, K.M. Lim, T.E. Tay, Molecular dynamics simulations on the inhibition of cyclin-dependent kinases 2 and 5 in the presence of activators, J. Comput. Aided Mol. Des. 20 (2006) 395–404.
[14] D.C. Li, B.H. Ji, K. Hwang, Y.G. Huang, Crucial roles of the subnanosecond local dynamics of the flap tips in the global conformational changes of HIV-1 protease, J. Phys. Chem. B 114 (2010) 3060–3069.
[15] V. Tozzini, J.A. McCammon, A coarse grained model for the dynamics of flap opening in HIV-1 protease, Chem. Phys. Lett. 413 (2005) 123–128.
[16] C.A. Chang, J. Trylska, V. Tozzini, J.A. McCammon, Binding pathways of ligands to HIV-1 protease: coarse-grained and atomistic simulations, Chem. Biol. Drug Des. 69 (2007) 5–13.
[17] S. Spinelli, Q.Z. Liu, P.M. Alzari, P.H. Hirel, R.J. Poljak, The three-dimensional structure of the aspartyl protease from the HIV-1 isolate BRU, Biochimie 73 (1991) 1391–1396.
[18] J. Wang, P. Cieplak, P.A. Kollman, How well does a restrained electrostatic potential (resp) model perform in calculating conformational energies of organic and biological molecules, J. Comput. Chem. 21 (2000) 1049–1074.
[19] E.C. Meng, B.K. Shoichet, I.D. Kuntz, Automated docking with grid-based energy evaluation, J. Comput. Chem. 13 (1992) 505–524.
[20] D.A. Case, et al., AMBER 8, University of California, San Francisco, 2004.
[21] H.J.C. Berendsen, J.P.M. Postma, W.F. van Gunsteren, A.D. Nola, J.R. Haak, Molecular dynamics with coupling to an external bath, J. Chem. Phys. 81 (1984) 3684–3690.
[22] G.D. Hawkins, C.J. Cramer, D.G. Truhlar, Pairwise solute descreening of solute charges from a dielectric medium, Chem. Phys. Lett. 246 (1995) 122–129.
[23] G.D. Hawkins, C.J. Cramer, D.G. Truhlar, Parametrized models of aqueous free energies of solvation based on pairwise descreening of solute atomic charges from a dielectric medium, J. Phys. Chem. 100 (1996) 19824–19839.
[24] V. Tsui, D.A. Case, Theory and applications of the generalized Born solvation model in macromolecular simulations, Biopolymers (Nucl. Acids Sci.) 56 (2001) 275–291.
[25] D. Sitkoff, K.A. Sharp, B. Honig, Accurate calculation of hydration free energies using macroscopic solvent models, J. Phys. Chem. 98 (1994) 1978–1988.
[26] J. Weiser, P.S. Shenkin, W.C. Still, Approximate atomic surfaces from linear combinations of pairwise overlaps (LCPO), J. Comput. Chem. 20 (1999) 217–230.
[27] N.A. Baker, D. Sept, S. Joseph, M.J. Holst, J.A. McCammon, Electrostatics of nanosystems: application to microtubules and the ribosome, Proc. Natl. Acad. Sci. U.S.A. 98 (2001) 10037–10041.
[28] T.J. Dolinsky, J.E. Nielsen, J.A. McCammon, N.A. Baker, PDB2PQR: an automated pipeline for the setup of Poisson–Boltzmann electrostatics calculations, Nucl. Acids Res. 32 (2004) W665–W667.
[29] M.F. Sanner, A.J. Olson, J.C. Spehner, Reduced surface: an efficient way to compute molecular surfaces, Biopolymers 38 (1996) 305–320.
[30] D. Sitkoff, K.A. Sharp, B. Honig, Accurate calculation of hydration free-energies using macroscopic solvent models, J. Phys. Chem. 98 (1994) 1978–1988.
[31] W. Wang, P.A. Kollman, Computational study of protein specificity: the molecular basis of HIV-1 protease drug resistance, Proc. Natl. Acad. Sci. U.S.A. 98 (2001) 14937–14942.
[32] V. Tozzini, J. Trylska, C.E. Chang, J.A. McCammon, Flap opening dynamics in HIV-1 protease explored with a coarse-grained model, J. Struct. Biol. 157 (2007) 606–615.
[33] M. Zacharias, Protein-protein docking with a reduced protein model accounting for side-chain flexibility, Protein Sci. 12 (2003) 1271–1282.
[34] D. Li, M. Liu, B. Ji, K. Hwang, Y. Huang, Coarse-grained molecular of ligands binding into protein: the case of HIV-1 protease inhibitors, J. Chem. Phys. 130 (2009) 215102.
[35] K. Wittayanarakul, S. Hannongbua, M. Feig, Accurate prediction of protonation state as a prerequisite for reliable MM-PB(GB)SA binding free energy calculations of HIV-1 protease inhibitors, J. Comput. Chem. 29 (2007) 673–685.
[36] N. Spackova, et al., Molecular dynamics simulations and thermodynamics analysis of DNA-drug complexes. Minor groove binding between 4¢, 6-diamidino-2-phenylindole and DNA duplexes in solution, J. Am. Chem. Soc. 125 (2003) 1759–1769.
[37] M. Lepsik, Z. Havlas, Efficiency of a second-generation HIV-1 protease inhibitor studied by molecular dynamics and absolute binding free energy calculations, Proteins 57 (2004) 279–293.
[38] E.J. Rodriguez, C. Debouck, I.C. Deckman, H. Abusoud, F.M. Raushel, T.D. Meek, Inhibitor binding to the Phe53Trp mutant of HIV-1 protease promotes conformational changes detectable by spectrofluorometry, Biochemistry 32 (1993) 3557–35563.
[39] K.W. Lexa, K.L. Damm, J.J. Quintero, J.E. Gestwicki, H.A. Carlson, Clarifying allosteric control of flap conformations in the 1TW7 crystal structure of HIV-1 protease, Proteins 74 (2009) 872–880.
[40] E.F. Pettersen, T.D. Goddard, C.C. Huang, G.S. Couch, D.M. Greenblatt, E.C. Meng, T.E. Ferrin, J. Comput. Chem. 25 (2004) 1605–1612.
[41] W. Humphrey, A. Dalke, K. Schulten, Vmd – visual molecular dynamics, J. Mol. Graph. Model. 14 (1996) 33–38.